Filamentation and Second-Harmonic Emission in Laser-Plasma Interactions

P. E. Young, H. A. Baldis, [a] T. W. Johnston, [b] W. L. Kruer, and K. G. Estabrook

University of California, Lawrence Livermore National Laboratory, Livermore, California 94550

(Received 13 October 1989)

Interferograms of an underdense, preformed plasma which is irradiated with a line-focused laser beam show pronounced density perturbations. The interferograms are compared to simultaneous, gated images of second-harmonic emission. We observe a correlation between the spatial positions of the density perturbations and the peak of the second-harmonic emission. We interpret these phenomena as being emission from a local, nonlinear focus in the underdense plasma, rather than from the entire length of a filament.

The filamentation instability[1] in laser-produced plasmas is of great interest because of its possible role in degrading the coupling of lasers to inertial-confinement-fusion targets. Filamentation has recently been studied extensively in numerical simulations[2-8] and experiments.[9,10] Filaments have been invoked to explain numerous experimental phenomena, one of which is the observation[11-14] of emission at the second harmonic of the incident laser frequency, ω_0, from underdense plasmas at angles perpendicular to the incident laser beam. No direct link between filaments and underdense $2\omega_0$ emission has been demonstrated to date, in part because there are numerous theoretical explanations for harmonic emission,[14,15] and in part because the density perturbations produced by filamentation have only recently been clearly identified.[9]

In this Letter, we will discuss experimental observations in which a short-pulse, high-intensity laser beam interacts with an underdense plasma formed by another laser pulse, and produces a density perturbation which can be detected interferometrically. A fast-framing camera simultaneously records the image of the $2\omega_0$ emission. This allows a simple comparison between the spatial positions of the density perturbation and the second-harmonic emission. The main result of this Letter is that $2\omega_0$ emission is spatially correlated with the density perturbations, but is not observed for the entire length of the filament.

Our experiment was conducted using two beams of the Chroma laser at KMS Fusion. One beam irradiated a thin foil target (0.35-μm-thick CH) at an angle 50° from the target normal to form a plasma. This laser pulse was nominally square with a 500-ps duration, and had an energy of 65 J and a wavelength of 1.06 μm. The laser spot on target was circular with a diameter of 450 μm. The foil burned through approximately 300 ps into the laser pulse and eventually formed a plasma that was nearly symmetric about both the plane of the target and the laser axis.

A second, short-pulse beam, which we will call the interaction beam, was delayed relative to the falling edge of the first pulse by 300 ps. The interaction-beam wavelength was also 1.06 μm; the pulse was Gaussian with a

100-ps FWHM, and had a laser energy of 35 J. The interaction beam was focused to a line by a positive spherical ($f/6$) lens with a negative cylindrical lens placed just before it. At best focus, the beam had dimensions of 50×250 μm^2, which was verified by imaging the transmitted beam at the target plane. The position of best focus was varied between target irradiations by moving the spherical focusing lens. The polarization of this beam was linear and tilted with respect to the horizontal plane by 45°.

A single-frame holographic imaging system[16] recorded the line integral of the phase shift of a probe beam which passed through the plasma, tangential to the target plane. The probe beam had a wavelength of 0.25 μm, was a Gaussian pulse of 20-ps duration, and was aligned parallel to the line focus of the interaction beam. The probe-beam pulse arrived at the target at the same time as the interaction beam. Because the interaction beam is focused to a line, rather than a circular spot, it is possible to see a large phase shift [see Fig. 1(a)] even if the density perturbation produced by the interaction beam is small.[9,10]

The other important diagnostic in this experiment is a gated optical imager (GOI)[17] which is a single-frame framing camera with 120-ps gate width. The target was imaged onto the camera by a single-element lens ($f/6$) which viewed the plasma from the side opposite to the holographic imager, and at an angle of 5° in front of the target relative to the probe beam. The light from the plasma was spectrally filtered to provide $\sim 10^{-6}$ attenuation of emission outside a wavelength window of $\lambda = 5320 \pm 100$ Å. The GOI was gated at the same time that the interaction beam reached the target. Because of the short gate width, all of the $2\omega_0$ emission shown in this Letter [see Figs. 1(b) and 2(b)] is due to the interaction beam, not the plasma-forming beam. The time resolution of the GOI simplifies the interpretation of the images compared to time-integrated measurements[11] and minimizes blurring due to plasma motion.

In Figs. 1 and 2, we compare the simultaneous interferograms and the GOI pictures from two target irradiations. The object plane for both diagnostics was located midway into the plasma. By imaging a 400-μm-diam
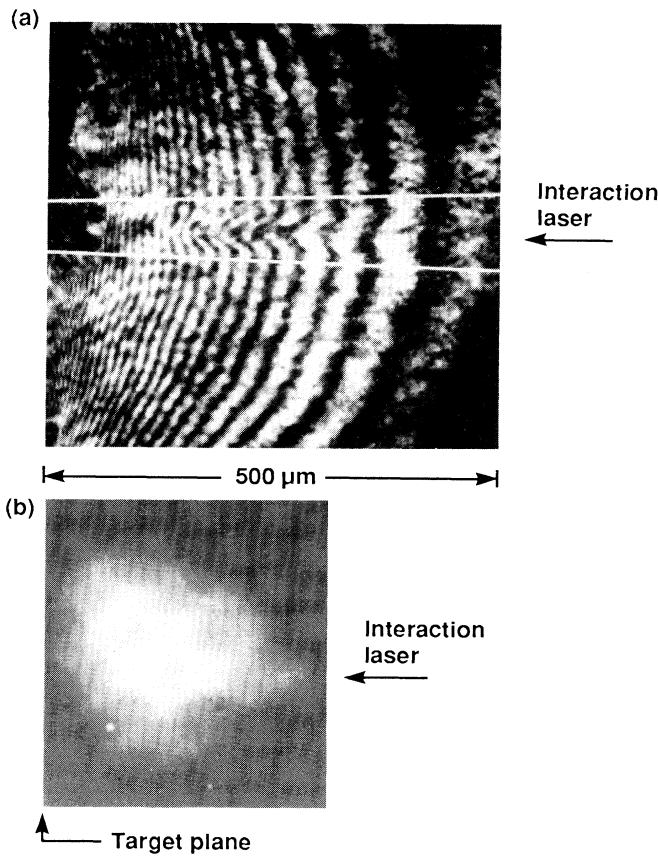
© 1989 The American Physical Society

FIG. 1. Comparison of (a) an interferogram and (b) a 120-ps gated image of a plasma with the best focus of a line focus located at the target plane. The pictures are recorded at the same time and only the side of the plasma facing the laser (incident from the right) is shown. The white lines in (a) show the estimated path of the $1/e$ level of the intensity profile of the interaction beam without the plasma.

FIG. 2. Comparison of (a) an interferogram and (b) a 120-ps gated image of a plasma with the best focus of a line focus located 400 μm in front of the target plane.

steel ball onto both diagnostics we can reconstruct images with the same magnification. The three small spots seen in the lower half of the GOI pictures are defects in the microchannel plate which reference the position of the second-harmonic emission on any shot relative to the target plane. The target plane in the interferograms is well defined by the shadow of the washer that supports the CH foil [left side of Figs. 1(a) and 2(a)].

For the target irradiation of Fig. 1, the best focus of the interaction beam was positioned at the target plane. The interferogram shows a density perturbation which is centered vertically and extends between 150 and 400 μm in front of the target. Subsequently, the spherical focusing lens was moved 400 μm away from the target to produce the data shown in Fig. 2. Once again there is a density perturbation centered vertically but with a smaller horizontal extent. These two figures show that the peak of the $2\omega_0$ emission moves as well.

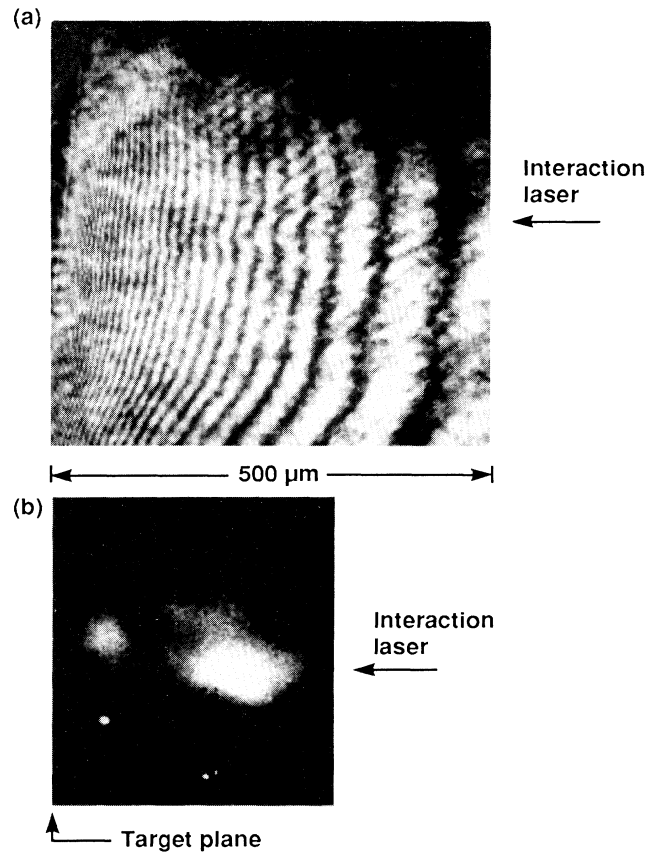From the interferogram, we can deconvolve the back-

ground density with the assumption of axial symmetry, by using an Abel-inversion routine while neglecting the phase shift due to the line-focus density perturbation. This gives the density profile in the central plane of the plasma which passes through the laser axis. This profile is then corrected for the density perturbation produced by the line-focused interaction beam by noting that the phase shift, $\Delta\phi$, of the probe beam through the line focus is related to the density perturbation δn by

$$\Delta\phi = 9 \times 10^{-22} \pi L_{p,\mu} \lambda_{p,\mu} \delta n , \tag{1}$$

where $\lambda_{p,\mu}$ is the wavelength of the probe beam in μm, $L_{p,\mu}$ is the path length through the plasma in μm, and δn has units of cm^{-3}. We will take $L_{p,\mu}$ to equal the length of the line focus ($=250$ μm) to get $\delta n = 6 \times 10^{18} \Delta\phi$, which we subtract from the unperturbed density profiles (dotted lines) to get the density profiles (dashed lines) shown in Fig. 3.

The density perturbation given by simple pressure balance between the laser and the plasma can be calculated from Eq. (2) of Ref. 9; for plasma parameters of $T_e \sim 500$ eV (from simulations), $n/n_c = 0.1$, and $I_L = 1.3$
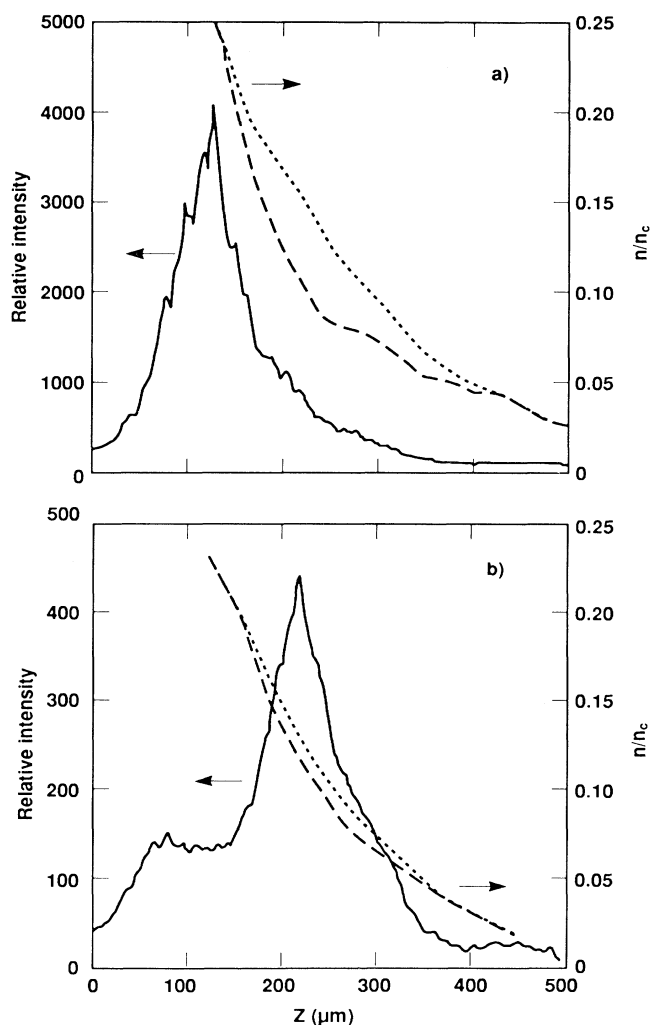
FIG. 3. Comparison of density profiles (obtained by unfolding the interferograms) with relative intensity contours of $2\omega_0$ light (solid lines). Shown are density profiles along the laser axis with (---) and without ($\cdots$) the perturbation produced by the interaction beam. The profiles are obtained from the data for the cases shown (a) in Fig. 1, and (b) in Fig. 2.

$\times 10^{15}$ W/cm^2, we calculate $\delta n/n \simeq 30\%$. The observation in this experiment that the perturbations have a finite axial extent suggests, however, that the laser light is self-focusing (and, subsequently, defocusing). The size of the initial density perturbation is large enough that predicted filamentation focusing lengths based on small initial perturbations[10,18] are not applicable. One can integrate the equation of refraction of a light ray[19] and define the self-focusing length l_{SF} to be the distance required to deflect a ray at the radius of the hot spot, $r = r_0$, to $r = 0$. Using the equation for ponderomotive pressure balance we find

$$l_{SF} = \alpha \frac{\omega_0}{\omega_{pe}} \frac{v_e}{v_{0s}} r_0, \qquad (2)$$

where ω_{pe} is the electron plasma frequency, v_e is the electron thermal velocity, and v_{0s} is the electron oscillatory velocity in the light wave. The dimensionless parameter α is selected, based on numerical simulations of the nonlinear Schrödinger equation,[20] to be $\alpha = 1.7$. For the plasma parameters listed above, with an initial beam radius of 50 μm, we find $l_{SF} \simeq 250$ μm, which is in good agreement to the observed focusing distance (from the edge of the plasma to the maximum density perturbation). The inverse bremsstrahlung absorption length is calculated to be (for $Z = 3.5$) > 4 mm, which is too large to explain the finite axial extent of the density perturbation.

Our calculations with a saturable (exponential) nonlinearity suggest that as the laser beam self-focuses, it develops substructure and collapses into a number of filaments. In 3D calculations, these filaments become very intense and small (a radius of only several wavelengths). The resulting strong gradients in intensity and density enhance the $2\omega_0$ emission. However, ion waves are expected to be generated in the final, nonadiabatic stage of the formation of such intense, narrow filaments. These ion waves can provide density modulations which act to delocalize or spray the filaments.[3,5]

We have converted the recorded film density of the $2\omega_0$ emission to relative intensity and compared these profiles along the laser axis to the density profiles for the two cases discussed: Figure 3(a) is for the interaction-beam focus at the target plane, as seen in Fig. 1, and Fig. 3(b) is for the interaction-beam focus 400 μm in front of the target plane, as seen in Fig. 2. The peak of the $2\omega_0$ emission occurs in or near the density perturbation in both cases, probably at the position of the peak incident intensity. The difference in position of the $2\omega_0$ emission relative to the filament is probably due to the dynamics of the self-focusing process; in Fig. 1 the beam is converging in the plasma while in Fig. 2 the beam is diverging. Refraction of $2\omega_0$ rays propagating through the filament, combined with the large extent of the radiating object compared to the depth of focus of the imaging lens, is probably responsible for the vertical and horizontal extent of the $2\omega_0$ emission seen in the images [particularly Fig. 1(a)].

While our results are generally consistent with previous explanations[11,13] of $2\omega_0$ emission from underdense plasmas and with the belief that this happens in filaments, these time-resolved results show the importance of the filamentary focus as the chief source of emission, rather than emission along the length of the filament. The source term is proportional to $E_0(\mathbf{E}_s \cdot \nabla)n + E_s(\mathbf{E}_0 \cdot \nabla)n$, where E_0, E_s are the incident and scattered laser lights, respectively. Hence, in a uniform filament one expects the $2\omega_0$ source to be localized at the filament edge along the length of the filament. Experimentally one sees a laterally diffuse $2\omega_0$ source concentrated near the end of the measured filament, presumably the focus. There one expects ∇n no longer to have

strict transverse symmetry, and to be quite large, with E_s likely not in a backscatter collimated direction. All of this should allow a considerable relaxation of constraints on $2\omega_0$ emission direction and polarization. Investigation of these and other spectral features is left to future work. It is likely that the z extension observed in time-integrated images[11] (for long laser pulses) is largely due to focus motion.

In conclusion, we find that there can indeed be a correlation between second-harmonic emission and density perturbations produced by a laser beam interacting with an underdense plasma. Although we have demonstrated experimental conditions in which $2\omega_0$ is associated with filaments, the use of $2\omega_0$ as a diagnostic for filamentation in underdense plasmas is problematic, because (i) the $2\omega_0$ emission does not show the complete extent of the filaments (see Figs. 1–3), (ii) significant $2\omega_0$ emission is observed only at high intensities (we do not observe significant $2\omega_0$ from filaments for the conditions of Ref. 9), and (iii) the $2\omega_0$ emission does not give a quantitative measurement of $\delta n/n$. The unambiguous way to study filamentation is with direct measurement of the density perturbation, i.e., using interferometry or schlieren.

(a)Permanent address: National Research Council of Canada, Ottawa, Ontario, Canada K1A 0R6.

(b)Permanent address: Institut National de la Recherche Scientifique–Energie, Varennes, Quebec, Canada J3X 1S2.

[1] P. K. Kaw, G. Schmidt, and T. Wilcox, Phys. Fluids **16**, 1522 (1973).

[2] R. S. Craxton and R. L. McCrory, J. Appl. Phys. **56**, 108 (1984); K. Estabrook et al., Phys. Fluids **28**, 19 (1985).

[3] R. D. Jones et al., Phys. Fluids **31**, 1249 (1988).

[4] R. Rankin et al., Phys. Fluids **31**, 2327 (1988).

[5] S. V. Coggeshall et al., Phys. Fluids **31**, 2750 (1988).

[6] A. J. Schmitt, Phys. Fluids **31**, 3079 (1988).

[7] R. H. Lehmberg et al., J. Appl. Phys. **62**, 2680 (1987).

[8] D. Havazelet et al., Phys. Fluids B **1**, 893 (1989).

[9] P. E. Young et al., Phys. Rev. Lett. **61**, 2336 (1988).

[10] P. E. Young, Comments Plasma Phys. Controlled Fusion **12**, 53 (1988).

[11] J. A. Stamper et al., Phys. Fluids **28**, 2563 (1985).

[12] J. Meyer and Y. Zhu, Phys. Fluids **30**, 890 (1987).

[13] A. Giulietti et al., Phys. Rev. Lett. **63**, 524 (1989).

[14] N. G. Basov et al., Kvantovaya Elektron. **6**, 1829 (1979) [Sov. J. Quantum Electron. **9**, 1081 (1979)].

[15] T. Weihan and G. Min, Laser Part. Beams **7**, 131 (1989).

[16] Gar. E. Busch et al., Rev. Sci. Instrum. **56**, 879 (1985).

[17] P. E. Young et al., Rev. Sci. Instrum. **59**, 1457 (1988).

[18] W. L. Kruer, Comments Plasma Phys. Controlled Fusion **9**, 63 (1985).

[19] K. Estabrook et al., Phys. Fluids **28**, 19 (1985).

[20] B. F. Lasinski and A. B. Langdon, Laser Program Annual Report— 1979, Lawrence Livermore National Laboratory, Livermore, CA, Report No. UCRL-50021-79, 1980 (unpublished), pp. 3–47.

(a)

Interaction laser

|← ——————— 500 μm ——————— →|

(b)
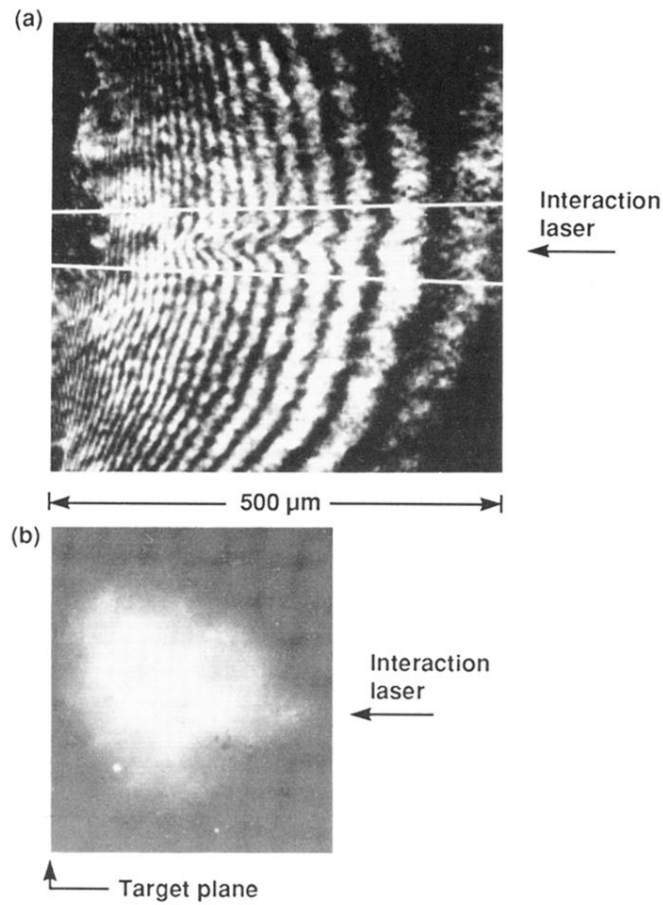
Interaction laser

↑— Target plane

FIG. 1. Comparison of (a) an interferogram and (b) a 120-ps gated image of a plasma with the best focus of a line focus located at the target plane. The pictures are recorded at the same time and only the side of the plasma facing the laser (incident from the right) is shown. The white lines in (a) show the estimated path of the 1/e level of the intensity profile of the interaction beam without the plasma.
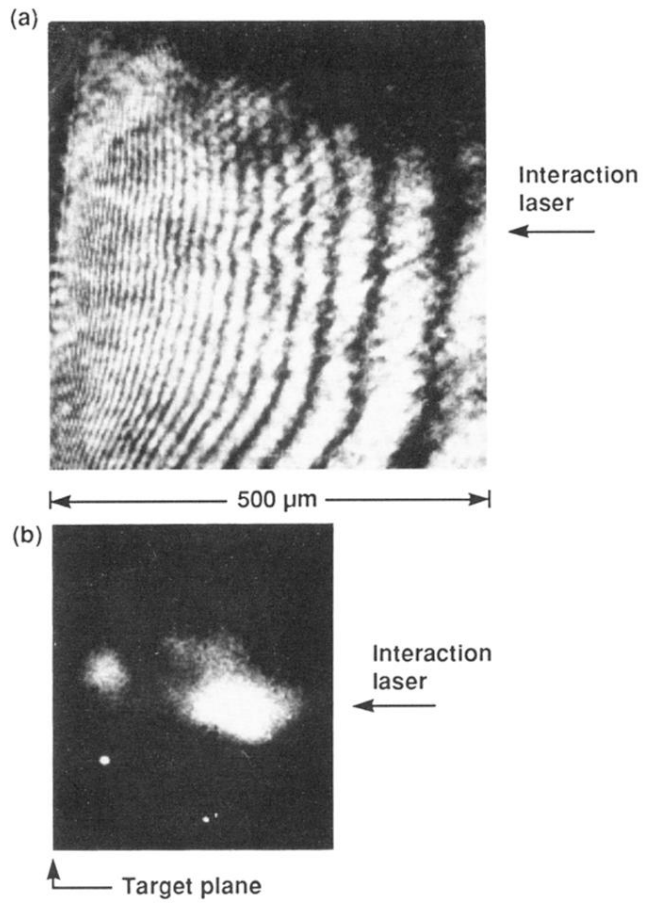
FIG. 2. Comparison of (a) an interferogram and (b) a 120-ps gated image of a plasma with the best focus of a line focus located 400 μm in front of the target plane.